Neuron
Article

# Endogenous Electric Fields May Guide Neocortical Network Activity

Flavio Fröhlich[1] and David A. McCormick[1,*]
[1]Department of Neurobiology, Kavli Institute of Neuroscience, Yale University School of Medicine, 333 Cedar Street, New Haven, CT 06510, USA
*Correspondence: david.mccormick@yale.edu
DOI 10.1016/j.neuron.2010.06.005

## SUMMARY

**Local field potentials and the underlying endogenous electric fields (EFs) are traditionally considered to be epiphenomena of structured neuronal network activity. Recently, however, externally applied EFs have been shown to modulate pharmacologically evoked network activity in rodent hippocampus. In contrast, very little is known about the role of endogenous EFs during physiological activity states in neocortex. Here, we used the neocortical slow oscillation in vitro as a model system to show that weak sinusoidal and naturalistic EFs enhance and entrain physiological neocortical network activity with an amplitude threshold within the range of in vivo endogenous field strengths. Modulation of network activity by positive and negative feedback fields based on the network activity in real-time provide direct evidence for a feedback loop between neuronal activity and endogenous EF. This significant susceptibility of active networks to EFs that only cause small changes in membrane potential in individual neurons suggests that endogenous EFs could guide neocortical network activity.**

## INTRODUCTION

Structured neocortical neuronal activity generates fluctuations in extracellular potential that are routinely recorded as local field potentials (LFPs) and electroencephalograms (EEGs) (Freeman, 1975; Mitzdorf, 1985; Nunez and Srinivasan, 2006). The study of these network-level signals is gaining momentum (Berens et al., 2008; Buzsáki, 2006; Katzner et al., 2009) since they carry important information about cognitive and behavioral states (Fries et al., 2001, 2008; Gail et al., 2004; Liu and Newsome, 2006; Pesaran et al., 2002; Riedner et al., 2007; Schroeder et al., 1998; Spinks et al., 2008; Taylor et al., 2005; Wilke et al., 2006) and provide insight into aberrant network dynamics associated with central nervous system disorders (Niedermeyer and Lopes da Silva, 2005).

Do these endogenous electric fields (EFs) directly influence neuronal behavior? Indeed, EFs can depolarize neurons (Jefferys, 1995). However, little is known about the effect of weak EFs with amplitudes as they occur in vivo. Interestingly, hyperexcitable and pharmacologically activated rodent hippocampal networks were recently found to be susceptible to very weak EFs (Deans et al., 2007; Francis et al., 2003). It is unknown if these findings generalize to neocortex with less structural stereotypy and lower cell densities in comparison to rodent hippocampus. Nevertheless, these findings are suggestive of the endogenous EF being more than just a mere epiphenomenon of network activity.

We hypothesize that endogenous neocortical EFs directly affect the neurons in the network that generates these fields. In this framework, population activity and its endogenous EF form a feedback loop: activity fluctuations cause a change in the endogenous EF that in turn affects the membrane voltage of the neurons that generate the population activity. Macroscopic electric activity may thus represent a dynamic feedback mechanism that modulates and guides neuronal circuit activity. In the case of neuronal oscillations, such a proposed global feedback signal could serve as a network-wide synchronization signal that enhances the spatiotemporal structure of network activity.

In this study, we investigated the existence and potential role of such a feedback loop in neocortex. We ask (1) if neocortical networks that exhibit physiological network activity are susceptible to weak EFs and (2) if feedback interaction between ongoing network activity and its corresponding EF has an effect on the network dynamics.

## RESULTS

### Neocortical Slow Oscillation Causes an Endogenous Electric Field In Vivo

We first characterized the spatiotemporal endogenous EF pattern caused by structured neocortical activity in vivo. Network activity in primary visual cortex of anesthetized ferrets robustly exhibited the slow oscillation (Haider et al., 2006; Steriade and Amzica, 1996; Steriade et al., 1993) that is characterized by periodic fluctuations in the LFP that reflect alternating epochs of multiunit neuronal firing (Up state) and quiescence (Down state; Figure 1A). We simultaneously recorded the LFP with multisite depth-electrodes (Figure 1B, left) and computed the EF strength between neighboring recording sites by taking the spatial derivative between them (Figure 1B, right). The slow oscillation is accompanied by a pronounced endogenous EF with a peak positive field strength in the superficial layers

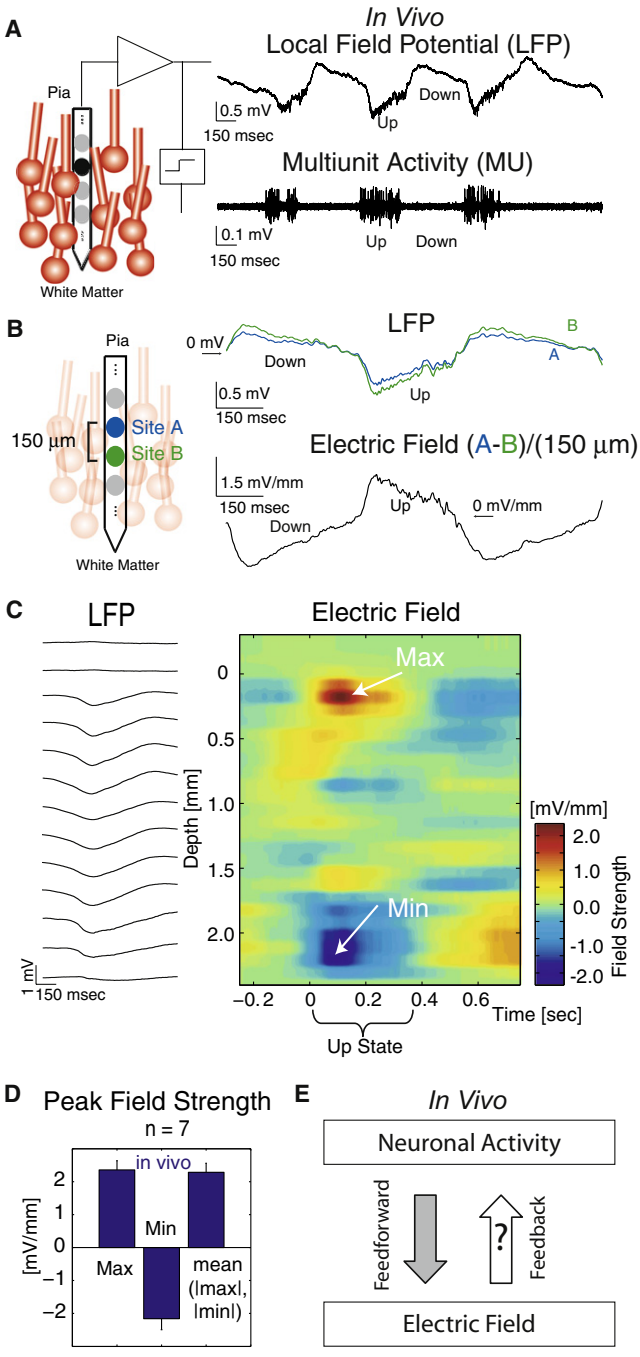


**Figure 1. Structured Neocortical Network Activity and Associated Endogenous EF**

(A) Extracellular recording in primary visual cortex in anesthetized ferrets exhibits the slow oscillation. Top: broadband LFP recording. Bottom: high-pass filtered multiunit activity. Network activity is structured into alternating epochs of activity and quiescence (Up and Down states).

(B) EF is the spatial gradient of the LFP determined from simultaneous multi-site recordings. Top: LFP traces of two neighboring electrodes (spacing: 150 µm). Bottom: corresponding EF.

(C) Sample experiment: LFP (left) and EF (right) exhibit spatiotemporal pattern that reflects the oscillatory nature of the ongoing network activity. Averaged traces are aligned on Up state initiation at time 0 s. Depth 0 mm corresponds to the most superficial electrode site where extracellular multiunit activity was first detected.

(D) Group data: maximum, minimum, and average of the absolute values of maximum and minimum EF peaks. Error bars here and below represent SEM.

(E) Conceptual framework: neuronal network activity generates an EF ("feedforward"). This EF in turn may influence neuronal activity ("feedback").

See also Figure S1.

and a peak negative field strength in the deep layers (Figure 1C). Across experiments, the median peak endogenous field strength amplitudes measured 2.36 ± 0.28 mV/mm and −2.16 ± 0.34 mV/mm for the maximal and minimal field strengths and 2.29 ± 0.27 mV/mm for the average absolute values of maximal and minimal field strength (median ± SEM, n = 7 array penetrations in 5 animals; Figure 1D). The strongest peak amplitude reached 3.89 mV/mm. These EFs are generated by the ion fluxes that underlie the synchronized neuronal activity (Figure 1E, "feedforward"). We hypothesize that these endogenous fields directly influence network activity by modulating neuronal membrane voltage (Figure 1E, "feedback") and thus form a feedback loop between neuronal activity and endogenous EF.

## Weak Electric Fields Cause Small Somatic Membrane Potential Depolarization

We took advantage of an in vitro slice preparation that spontaneously exhibits physiological activity (Up and Down states) to investigate the effect of weak EFs on active neocortical networks. Acute slices from ferret visual cortex, maintained in in vivo-like artificial cerebrospinal fluid (Sanchez-Vives and McCormick, 2000), spontaneously exhibit periodic, network-wide activity that resembles the neocortical in vivo slow oscillation (Figure 2A, top: lfp; bottom: multiunit activity). The endogenous field caused by slow oscillation in vitro (see Figure S1A available online) exhibited a structure similar to in vivo, but peak field strengths during the Up state of the slow oscillation were substantially smaller in vitro (Figure 2B; positive peak: 1.31 ± 0.15 mV/mm in vitro versus 2.36 ± 0.28 mV/mm in vivo, $p = 0.014$; negative peak: −0.47 ± 0.072 mV/mm in vitro versus −2.16 ± 0.34 mV/mm in vivo, $p < 0.001$; average absolute values of maximal and minimal field strength: 0.87 ± 0.095 in vitro versus 2.29 ± 0.27 in vivo, $p < 0.001$, n = 7 penetrations in 5 animals, n = 7 slices from 2 animals). Therefore, the in vitro preparation allows the application of external EF in the presence of spontaneous structured activity with reduced contamination from the endogenous EF in comparison to in vivo (Figure 2C). We applied external EFs with in vivo amplitudes through two parallel electrodes that lay on either side of the slice such that the field lines were approximately orthogonal to the cortical surface (Figures 2D and S2A). In order to assess the effect of externally applied fields, we combined extracellular multiunit array recordings with intracellular recordings (Figures 2D–2F).

First, we measured the effect of EFs with in vivo amplitudes on the membrane potential of individual neurons. Intracellular recordings from infragranular neurons (Figures 2G and 2H) showed a small net membrane voltage depolarization caused by application of constant EFs ($\Delta V_m$ = 0.49 ± 0.12 mV and $\Delta V_m$ = 1.29 ± 0.20 mV, for 2 and 4 mV/mm, respectively, $p < 0.001$ and $p < 0.001$, n = 11 cells). Thus, in agreement with

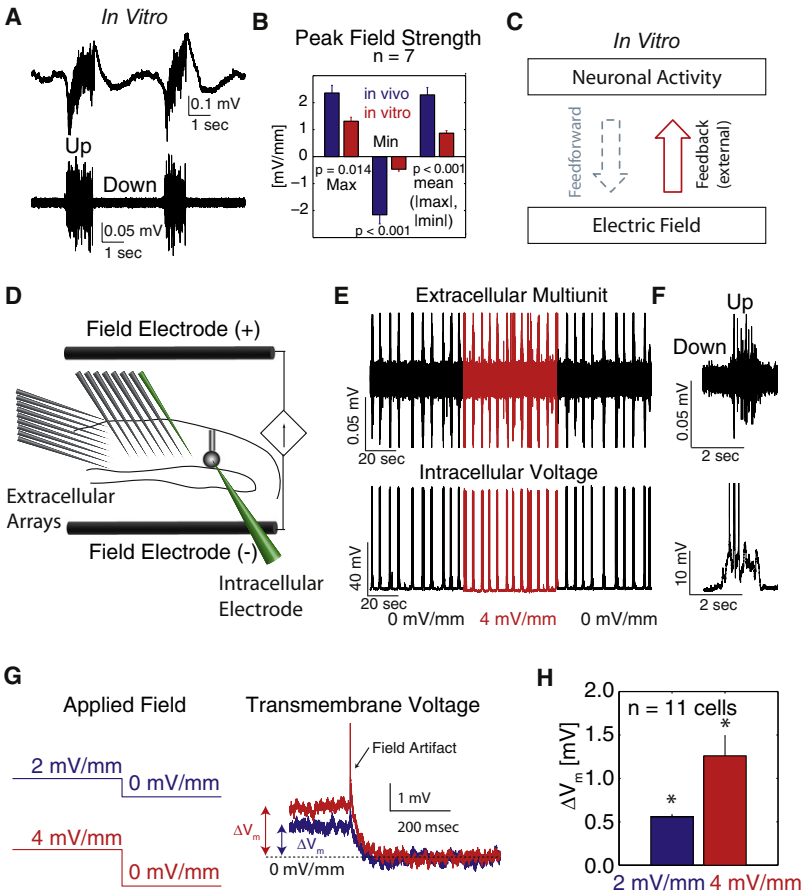


**Figure 2. Effect of Weak EF on Membrane Voltage**

(A) Slow oscillation in active neocortical slice. Top: LFP. Bottom: multiunit signal.

(B) Endogenous EFs. In vitro and in vivo group data for maximum, minimum, and average of the absolute values of maximum and minimum EF peaks for (all significantly different).

(C) In vitro, the endogenous EF generated by neuronal activity is considerably weaker ("feedforward") and thus facilitates the study of the "feedback pathway" in relative isolation by application of external EFs.

(D) External EF was generated by two parallel AgCl wires on the two sides of the slice such that field lines were orthogonal to the cortical layers. Change in transmembrane voltage was recorded by subsequent measurements of intra- and extracellular voltage with the same sharp glass microelectrode at the offset of constant field application.

(E) Simultaneous extracellular multiunit (top) and intracellular (bottom) recording of slow oscillation in vitro.

(F) Zoom-in on single Up state from (E). Intracellular recording truncated.

(G) Left: schematic representation of applied fields (2 mV/mm and 4 mV/mm). Right: averaged sample traces that show effect of 2 mV/mm and 4 mV/mm field on somatic transmembrane voltage. Vertical line represents field artifact from switching off field.

(H) Group data. Average change in transmembrane voltage $\Delta V_m$ for 2 and 4 mV/mm.

See also Figure S2.

recent hippocampal measurements (Deans et al., 2007), EFs with in vivo amplitudes caused small changes in somatic membrane potential of individual neurons. These small somatic depolarizations result from EF-mediated polarization of the neurons' elongated somatodendritic axis and the differences in field-induced distribution of charge within the neuron and the immediately adjacent extracellular space (Figures S2B–S2D). We next focused on how such small perturbations at the level of individual neurons affect the ongoing population activity. Specifically, we characterized the effect of EFs on active neuronal circuits by applying (1) constant, depolarizing fields, (2) sine-wave fields, (3) in vivo-like fields, (4) activity-dependent positive and negative "feedback" fields.

## Weak Constant Electric Fields Accelerate Neocortical Slow Oscillation In Vitro

We first applied constant, uniform EFs to the slices to establish that the slow oscillation can be modulated by an external EF similar in amplitude to the endogenous in vivo field. Specifically, network activity was monitored with two linear arrays of eight extracellular recording electrodes (one vertical spanning supra- to infragranular layers and one horizontal positioned in infragranular layers). Results were similar in all electrodes (data not shown) so we present data averaged across all recording locations except when studying the spatial network dynamics (Figures S3A and S3B). The application of a constant depolarizing external EF accelerated the slow oscillation frequency (reduced oscillation period) such that more Up states occurred within a given time interval (representative single experiment example: Figure 3A, top trace: multiunit activity without field applied; bottom trace: with 4 mV/mm field applied). Across experiments (n = 9), the slow oscillation period significantly decreased for both the 2 mV/mm and 4 mV/mm amplitude constant EFs (Figure 3B, left; decreased to 88% and 80% of control respectively, p = 0.02 and p = 0.0039). For constant fields with 0.5 and 1.0 mV/mm amplitude we found no significant effect (100% and 98% of control respectively, p = 0.55 and p = 0.81; not shown). This reduction in oscillation period for 2 and 4 mV/mm was due to a significant shortening of the duration of the Down state for both field strengths (Figure 3B, center; decreased to 86% and 77%, p = 0.0039 for both field amplitudes). Up state duration was not significantly modulated (Figure 3B, right; 102% and 100% of control, p = 0.36 and p = 0.65). For 2 and 4 mV/mm, Up state multiunit activity levels were slightly decreased by the applied field (decreased to 97% and 93% of control, p = 0.16 and p = 0.020; not shown) while Down state activity levels were elevated (increased to 107% and 133% of control, p = 0.098 and p = 0.020; not shown).

Given this enhancing effect of EFs on rhythmic neocortical activity, we next investigated whether the applied fields override or modulate the existing spatiotemporal network dynamics by examining the layer dependence of the Up state duration. Up states were longer in infragranular than in supragranular layers in absence of an external EF (supra: 0.67 ± 0.10 s and infra:

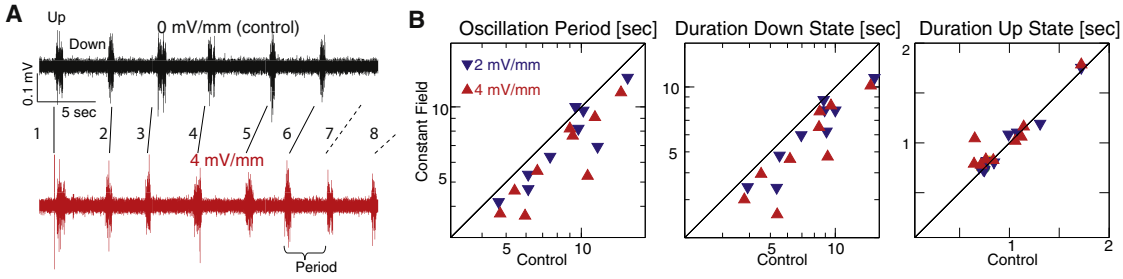


**Figure 3. Constant EF Enhances Slow Oscillation by Decreasing Oscillation Period and Shortening of Down States**

(A) Frequency of Up states increased in presence of constant field. Top: control. Bottom: with constant field. Up states are numbered to facilitate comparisons between conditions.

(B) Left: oscillation period is significantly decreased in presence of external field with 2 or 4 mV/mm amplitude. Middle: Down state duration is significantly decreased for 2 and 4 mV/mm. Right: Up state duration remains unaffected for all field amplitudes used (2.0 and 4.0 mV/mm shown).

See also Figure S3.

1.11 ± 0.17 s, p = 0.021, n = 9). This pattern was preserved in the presence of 2 mV/mm (supra: 0.61 ± 0.12 s; infra: 0.98 ± 0.12 s, p = 0.038, n = 9) and 4 mV/mm fields (supra: 0.59 ± 0.12 s; infra: 1.22 ± 0.31, p = 0.028, n = 9). Thus the applied EF modulates, rather than overrides, the "natural" network dynamics. Further support for this conclusion comes from the analysis of propagation delays (Figures S3A and S3B; representative examples) which showed little effect of applied fields on inter- and intralaminar propagation.

Since the applied EFs cause only small somatic depolarizations, we hypothesized that network interaction must play an important role in amplifying this weak yet global perturbation to the neurons in the network. To further elucidate this underlying mechanism, we experimentally isolated two orthogonal aspects of global modulation of network-wide activity by constant EFs (Figures S3D and S3E). First, we applied fields to individual neurons that were pharmacologically isolated from the network to demonstrate that neuronal firing rates are susceptible to the weak depolarizations when the membrane voltage is close to, or above, threshold. In these experiments, we blocked the slow oscillation by pharmacologically abolishing fast excitatory synaptic transmission and replaced the depolarizing drive with slow patterned DC injections that caused periodic firing in qualitative resemblance to Up states. We found that fields with both 2 and 4 mV/mm amplitudes caused a measurable increase in firing in comparison to control situation where no field was applied (Figures S3E and S3F; increased to 115% and 125% of control for 2 mV/mm and 4 mV/mm, respectively, p < 0.0005, n = 18). This result illustrates the importance of ongoing network activity, which brings neurons close to threshold, for weak EFs to have an effect. Second, we examined weak somatic depolarizations of individual cells induced by small amplitude intracellular DC injections (mimicking the effect of applied fields, causing somatic depolarizations smaller than 1.5 mV) during spontaneous slow oscillation (Figure S3G). We found an increase in firing during both Up and Down states (Figure S3H, top) and an advance of the firing of the injected cell during the Up state relative to the multiunit network activity (Figure S3H, bottom). Therefore, if a large number of neurons simultaneously receive such a weak depolarization (i.e., by the external field application), early transition into the next Up state may result (i.e., increase in oscillation frequency). These experiments demonstrate that the somatic depolarization induced by the field may serve as the underlying mechanism for the acceleration of the slow oscillation in response to DC field applications (Figure S7A–S7C).

## Weak Sine-Wave Electric Fields Entrains Slow Oscillation In Vitro

A key characteristic of the endogenous EF is its oscillatory structure during slow oscillation. We thus hypothesized that sine-wave EFs may have an effect on the timing and regularity of the ongoing network oscillation and thus change the autocorrelogram of the spiking network activity. Increases in overall activity levels are reflected in the central peak (CP) of the autocorrelogram and enhancement of the oscillatory structure causes an increased side-band peak (SB) at the oscillation period (SB/CP, normalized to the CP). Indeed, when we applied a sine-wave field that was approximately matched in oscillation period to the spontaneous network oscillation, we found that the slow oscillation became more periodic (Figure 4A, single experiment example). Accordingly, the autocorrelation of the multiunit spiking activity shows this enhancement of periodicity (Figure 4B; relative SB enhancement, black: control, red: applied field) with little change in overall activity levels (CP amplitude). We measured the change both in CP and in the SB/CP ratio for sine-wave fields approximately matched in oscillation frequency to the intrinsic oscillation with 0.5, 1.0, 2.0, and 4.0 mV/mm amplitudes. Across experiments, we found a striking increase in the oscillatory characteristic of the slow oscillation SB/CP for 1.0, 2.0, and 4.0 mV/mm (Figure 4D, right; median SB/CP ratios: 0 mV/mm: 0.12; 0.5 mV: 0.13, 1.0 mV/mm: 0.19, 2 mV/mm: 0.21; 4 mV/mm: 0.43; median SB/CP modulation indices: 0.5 mV/mm: 0.013 ± 0.042, p = 0.25, n = 9; 1.0 mV/mm: 0.18 ± 0.047, p = 0.020, n = 9; 2.0 mV/mm: 0.27 ± 0.065, p < 0.005, n = 10; 4.0 mV/mm: 0.53 ± 0.079, p < 0.005, n = 10). In addition, all fields with 1.0 mV/mm or higher amplitude caused a small but significant increase in CP for 1.0, 2.0, and 4.0 mV/mm (Figure 4C, left; median CP modulation index: 0.5 mV/mm: 0.015 ± 0.0078, p = 0.16, n = 9; 1.0 mV/mm: 0.021 ± 0.0090, p = 0.0078, n = 9; 2.0 mV/mm: 0.0435 ± 0.028, p = 0.02, n = 10; 4.0 mV/mm: 0.12 ± 0.050, p < 0.005, n = 10,

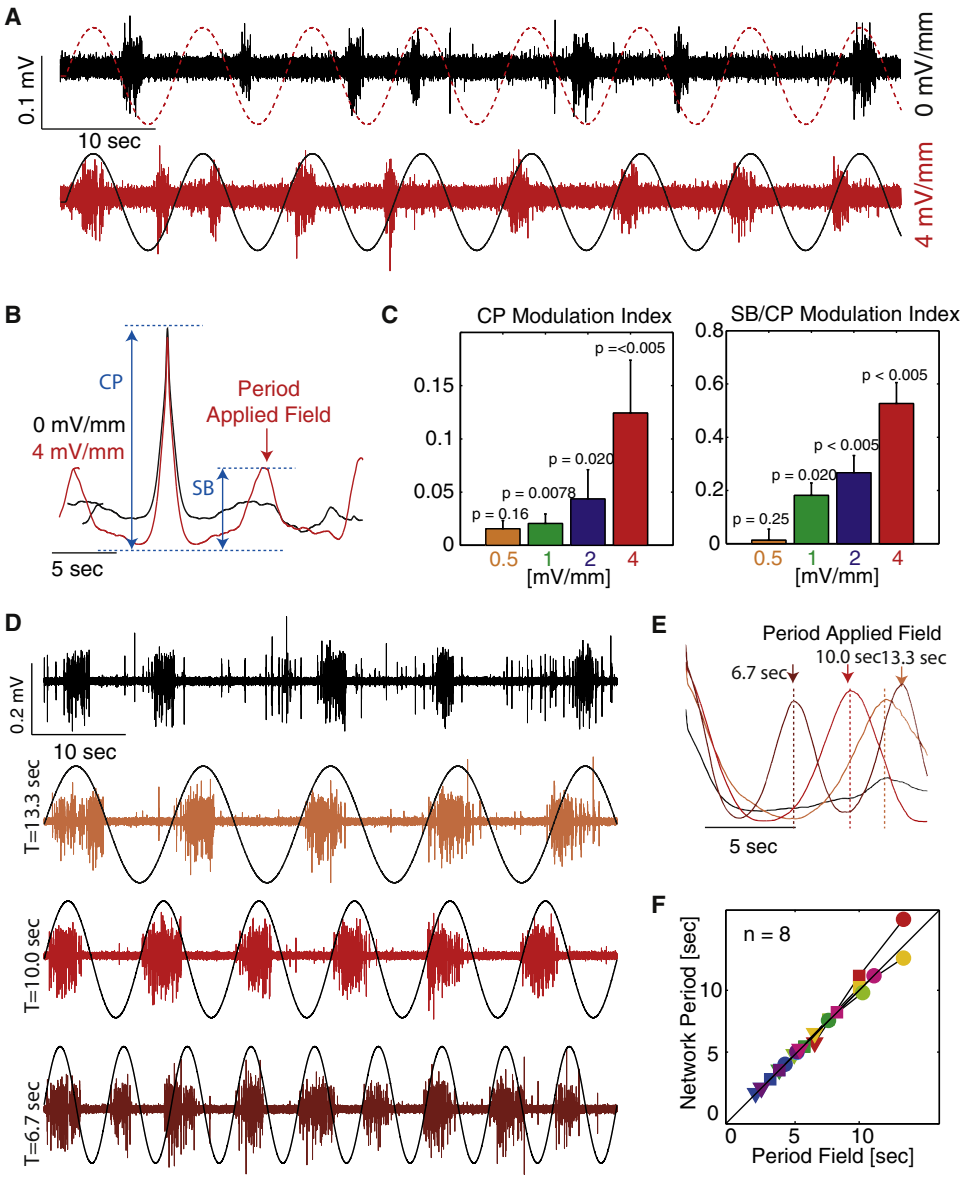


**Figure 4. Sine-Wave EFs Enhance Slow Oscillation**

(A) Multiunit recording in control condition (0 mV/mm; dashed line: "virtual extension" of field waveform) and with frequency-matched external sine-wave field (4 mV/mm).

(B) Autocorrelograms of multiunit firing reveal enhanced oscillatory characteristics during field application (enhanced sideband peak, SB). CP: central peak.

(C) Left: CP was significantly increased for fields with 1.0–4.0 mV/mm amplitude (median modulation index). Right: SB/CP was significantly increased for fields with 1.0–4.0 mV/mm amplitude (median modulation index).

(D) Sine-wave fields with three different periods (T) successfully entrained slow oscillation (top: control, top middle: T = 13.3 s, bottom middle: T = 10.0 s, bottom: T = 6.7 s).

(E) Correlograms show enhancement of oscillation at all field periods applied. Dashed lines mark SB peaks. Arrows indicate period of applied EFs.

(F) Across experiments, network period matched the period of the applied field (n = 8).

See also Figure S4.

definition in Experimental Procedures section). Together, these results suggest that frequency-matched oscillatory EFs mostly affect the temporal structure of the neural activity without major changes in the overall activity level. Similarly, we found that application of a 2 mV/mm sine-wave EF in vivo also modulated the slow oscillation, indicating that this effect is not limited to the in vitro condition (Figures S4B–S4D).

We next investigated sine-wave EFs with frequencies that did not match the intrinsic slow oscillation frequency. When we applied sine-wave EFs with different frequencies (0.075–0.375 Hz,

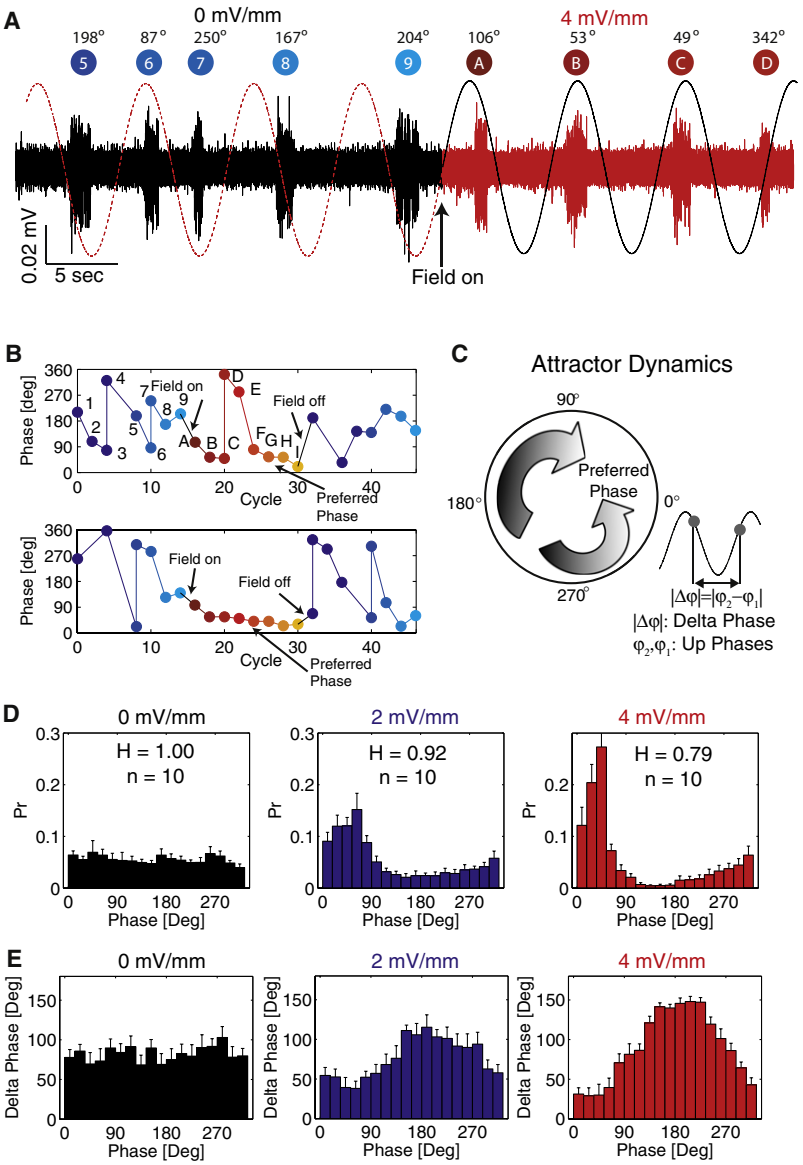


**Figure 5. Sine-Wave Field Entrains Up States**

(A) Left (black): slow oscillation in control condition (0 mV/mm; no applied field). Dashed line represents "virtual extension" of applied sine wave. Right (red): slow oscillation with sine-wave EF (4 mV/mm). Up states are marked with a label and their respective phases are shown.

(B) Representative examples of Up state phase as a function of cycle number of the Up state.

(C) Left: schematic representation of preferred phase as an attractor. If the phase assumes a value outside the basin of attraction for a given Up state (e.g., Up state "D"), the phases of the consecutive Up states rapidly change such that they converge back to preferred phase. Right: schematic representation of phase difference $|\Delta\varphi|$ as the absolute value of the difference between the two phases of two consecutive Up states.

(D) Up state phase distribution for control, 2 mV/mm, and 4 mV/mm applied sine wave fields (Pr: probability). Peak of phase histogram indicates preferred phase (n = 10). Normalized entropy H measures how uniform the phase distribution is.

(E) Absolute phase difference $|\Delta\varphi|$ of all consecutive Up state pairs ($\varphi_1$, $\varphi_2$) as a function of phase $\varphi_1$ is largest for values that are farthest from the preferred phase.

See also Figure S5.

set in each experiment to 2/3, 1/1, and 4/3 of estimated intrinsic network period) and 4 mV/mm amplitude the network adjusted its oscillation frequency to match the frequency of the applied field (Figure 4D). We determined the network oscillation period from the location of the first side-band peak in the multiunit autocorrelogram (Figure 4E, dotted lines: network oscillation period; arrows: period of applied fields). In the presence of the 4 mV/mm sine-wave field, the period of the network oscillation was very similar to the period of the applied field. Similar results were obtained across experiments, (Figure 4F, data points on unity line; n = 8). These results indicate that the applied sine-wave fields entrained the slow oscillation at the relatively broad range of frequencies that we examined. We next tested whether the strength of the entrainment varied as a function of frequency by comparing the SB/CP ratio as a function of the mismatch between the intrinsic and applied frequency. For 4 mV/mm, we found no clear relationship between how well the applied field frequency was matched to the intrinsic frequency and the resulting enhancement of the slow oscillation (Figure S4A, left; SB/CP ratio). In fact, the normalized oscillation enhancement as a function of the normalized mismatch between applied and intrinsic oscillation frequency showed no significant correlation for 4 mV/mm (R = 0.09, p = 0.18). However, a reduction of the amplitude of the applied field to 2 mV/mm (n = 8) caused a decrease in normalized oscillation enhancement for increased frequency mismatches (Figure S4A, right; blue, R = 0.31, p = 0.009). Together, these results show that (1) a sine-wave EF robustly entrains the slow oscillation and that (2) weaker EFs preferentially enhance the slow oscillation at its intrinsic frequency.

We next characterized the entrainment of the slow oscillation by analyzing the alignment of individual Up states with the applied sine-wave field. We measured the timing of the Up state onset relative to the applied sine-wave field by determining the phase of each Up state (Figure 5A; representative example; left: no field applied; right: field applied). For the control intervals, when no external field was applied, we extended the applied sine-wave as a "virtual" reference to determine the phase of the Up states in absence of an applied field (dashed red line in Figure 5A). We then tracked the Up state phase over time by plotting it as a function of the sequential number of the Up state (Figure 5B). The top example shows that Up state phases assumed a broad range of values before application of the field

but rapidly converged to a phase of around 45° when the field was applied. This evolution of the Up state phase suggests that there exists a preferred phase that the Up states assume in presence of an applied sine-wave field. Correspondingly, in the example shown, Up state "D" does not occur at the preferred phase but the phase reconverges back to the preferred Up state phase within the next two Up states ("E" and "F") and remains at the preferred phase for subsequent Up states ("G"–"I"). The bottom panel shows another trial from the same experiment where the phase converged to the preferred phase and remained there for the entire duration of the sine-wave field presentation. Once the sine-wave field application was removed, the tight phase relationship between the field and the slow oscillation was quickly lost (Figure 5B). System theory (Pikovsky et al., 2001) predicts that such a preferred phase should exist and assume the properties of an attractor in phase space (Figure 5C). We therefore next considered the group data to test (1) for the existence of such a preferred phase attractor and (2) the stability of the attractor.

To test for a preferred-phase attractor, we examined the distribution of all Up state phases during application of the sine-wave field and control epochs (Figure 5D). Clear peaks in these distributions indicate the existence of a preferred phase. We quantified the strength of the peak in these distributions by measuring the deviation from a uniform distribution by computing entropy H normalized to the entropy of a uniform distribution (values range from 1 for a uniform distribution to 0 for a deterministic process). We found uniform phase distributions in control without an applied field (population average, n = 10; Figure 5D, left; H = 1.00) and a clear peak in the phase distribution histogram during application of the sine-wave field (population average, n = 10; Figure 5D, middle and right; peaks at 70° and 50° with $H_{2mV/mm}$ = 0.92 and $H_{4mV/mm}$ = 0.79; p = 0.0098 and p = 0.002, n = 10). We also applied circular statistics to take the circular nature of phase measurements into account and to further confirm the significance of the peaks in the phase histograms (circular variance $S_{control}$ = 0.79, $S_{2mV/mm}$ = 0.51, $S_{4mV/mm}$ = 0.31 for control, weak, and strong field, respectively, p = 0.0098 and p = 0.0039, n = 10; Rayleigh test for nonuniformity significant with $p < 0.01$). These peaks in the phase histograms correspond to the preferred phase at which the Up state onset was most likely to occur and show that the enhancement of the ongoing slow oscillation by application of a sine-wave field is mediated by phase-locking of Up states to the applied oscillatory EF at the preferred-phase attractor.

We then investigated if the preferred-phase attractor is stable, i.e., (a) the Up state phase converges to the preferred phase upon application of the external field and (b) any deflection away from the preferred phase (e.g., due to noise) is followed by reconvergence to the preferred phase. We quantified the phase difference of consecutive Up states by computing the absolute value of the difference in their phase ($|\Delta\varphi|$; Figures 5C and 5E). This measure of phase difference assumes values between 0° and 180° (see also Experimental Procedures) and should converge to 90° on average in case of random alignment of Up states with a sinusoidal signal. If the preferred phase represents a stable attractor, $|\Delta\varphi|$ phase should be (1) low for Up states that exhibit phases similar to the preferred phase ("attractor reached") and (2) high for Up states with phases very different from the preferred phase (representing convergence back to the preferred phase). Across all experiments, we find this pattern. First, phase changes are least (small $|\Delta\varphi|$) for Up states with phases that correspond to the preferred phase (70° and 50° for 2 and 4 mV/mm, respectively). The deviations of $|\Delta\varphi|$ in our experiments from the theoretical zero value (when in phase with the sine-wave field) are a consequence of the inherent variability of Up state timing in cortical networks. In control without any field applied, the average phase difference indeed approaches the theoretical value of 90°. Second, phase changes are most (large $|\Delta\varphi|$) for Up states phase values that are around 180° offset to the preferred phase (Figure 5E). We further assessed the dependence of the phase difference on the phase in Figure 5E with the linear-circular association method to determine the correlation C between the circular phase variable $\varphi$ and the linear phase difference variable $|\Delta\varphi|$ (control: C = 0.047 with p = 0.0043; weak field: C = 0.32 with p = 0; strong field: C = 0.59 with p = 0, see also Experimental Procedures). These findings confirm that the preferred phase is a stable attractor.

## In Vivo Field Entrains Network In Vitro

In order to establish that modulation of network activity by EFs is not limited to waveforms with artificial temporal structure, we next applied a naturalistic EF waveform, which we had recorded in vivo to neocortical slices in vitro (n = 7). The peak strength of this applied field was adjusted to be approximately 4 mV/mm. We found that application of a temporally naturalistic field strongly modulated the ongoing activity of the local cortical network (Figure 6A; excerpt from sample experiment; left: control; right: in vivo field applied). In agreement with the sine-wave experiments, positive deflections in the applied field enhanced and guided multiunit activity (Figures 6B and 6C). To determine the field-amplitude sensitivity of the network activity, we plotted normalized enhancement of the multiunit activity as a function of the instantaneous field strength. This plot is flat for the control case where no field was applied (Figure 6D, black). When the in vivo field was applied (Figure 6D, red), there is an exponentially growing enhancement of the activity for increasing field strengths. The EF had a significant effect at 0.5 mV/mm (0.5 mV/mm, $p < 0.005$, n = 7), indicating that the threshold level for EF effects in vitro is between 0.25 and 0.5 mV/mm. These results illustrate that a low amplitude EF with a temporally naturalistic in vivo waveform can modulate ongoing network activity. Importantly, the in vivo waveform contained steeper slopes (i.e., higher frequency components) than the sine-wave EFs. We hypothesized that these steeper slopes entrain the network particularly well. Such a dependence on slope would explain the more pronounced effect at weaker amplitudes in case of the in vivo field in comparison to the sine-wave fields. Indeed, the response EF ramps with larger slopes but identical peak values showed higher multiple unit averages across trials (Figure S6A, top: applied field ramps, bottom: sample multiunit trace; Figure S6B; average multiunit response for all slopes tested; Figure S6C; normalized peak amplitude is higher for 8 and 4 mV/(mm*s) than for 0.5 mV/(mm*s), $p < 0.05$, one-sided ANOVA). Since applied fields in the amplitude range used in

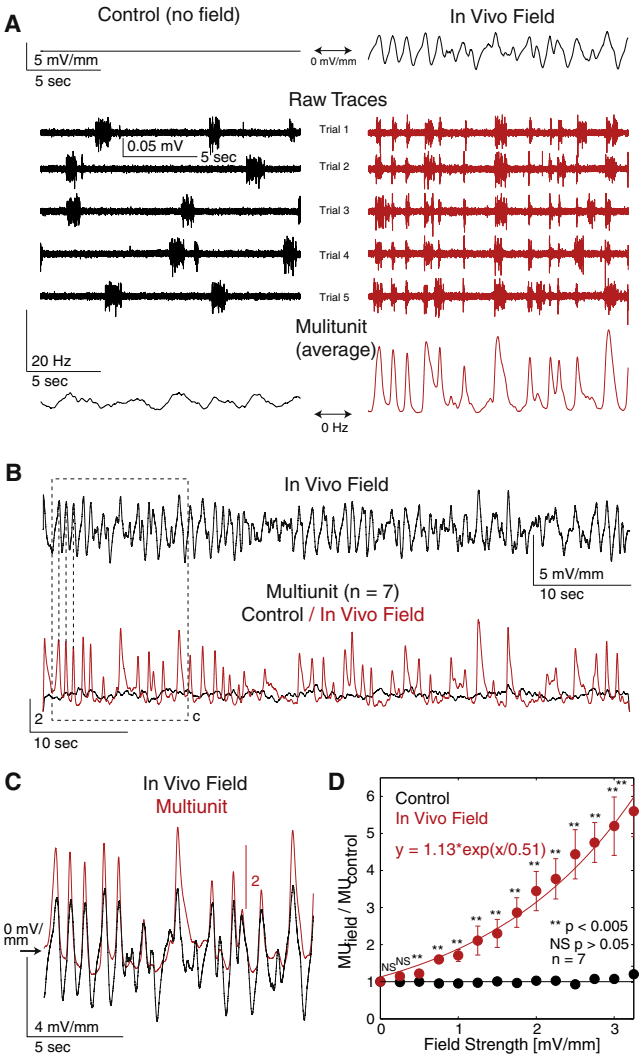


**Figure 6. In Vivo Field Waveform Guides Network Activity In Vitro**

(A) Time excerpt from representative example experiment. Left: control condition (no field applied). Right: in vivo field applied. Top: applied field waveform. Middle: multiunit traces from consecutive trials. During control periods, Up states occur at random points in time. In presence of in vivo field, Up states occur preferentially aligned with applied field waveform. Bottom: multiunit activity averaged across all trials. From 20 to 30 trials were applied of each waveform.

(B) Top: applied in vivo field waveform (duration: 60 s). Bottom: multiunit activity averaged across experiments for control condition (black) and for condition with in vivo field (red). Multiunit activity is normalized to the average activity level during control epochs.

(C) Zoom in from panel (B) as indicated by dashed box. Averaged multiunit (red) and applied EF (black).

(D) Relative enhancement of the instantaneous multiunit activity as a function of the instantaneous applied field strength (binned in 0.25 mV/mm intervals). Population average across experiments (n = 7). Black: control. Red: in vivo field applied, fitted with exponential function. Curves significantly diverge for field strengths of 0.50 mV/mm and higher (all points $p < 0.005$).

See also Figure S6.

this study do not succeed in bringing cells from rest to threshold but rather modulate the time of occurrence of individual Up states, faster (and thus shorter) ramps provide a more limited time window of opportunity for an Up state to occur. Therefore, across trials, Up states align better for fields with higher temporal derivatives (i.e., in vivo waveform and faster ramps) and result in higher temporal precision and thus higher multiunit peak amplitudes on average.

## Activity-Dependent Electric Fields Modulate Recurrent Network Activity In Vitro

So far, our results are highly suggestive of the existence of a feedback loop between structured neuronal activity and the endogenous EF. In order to more directly establish the existence of this proposed feedback interaction, we performed in vitro experiments where we provided simulated real-time EFs computed from the ongoing network activity (Figure 7A; set-up with sample multiunit activity trace and corresponding simulated EF traces). We used positive and negative activity-dependent EF waveforms to provide positive and negative feedback, respectively. In case of the positive feedback, this set-up approximates the in vivo case where the ongoing neuronal activity generates a pronounced endogenous EF. This experimental configuration enables us to directly compare network dynamics with and without this positive feedback mechanism present. We found that adding this positive feedback mechanism enhances the oscillatory nature of the structured network activity. A comparison of the multiunit activity in the control (Figure 7B, black) and feedback condition (Figure 7B, red) in a representative example shows that the Up states occurred at more regular intervals with the positive feedback mechanism present. The enhanced periodicity of the slow oscillation is reflected by an increased first SB and CP in the autocorrelogram (Figure 7C, black: control; red: with feedback). Similarly, both CP (Figure 7D, left; median increase to 120% of control, $p = 0.016$) and normalized SB amplitude (Figure 7D, right, SB/CP, median increase to 150%, $p = 0.031$) were enhanced in the group data ($n = 7$). We then measured the cycle-to-cycle variability of the slow oscillation by calculating the coefficients of variation (std/mean) of both the Up and the Down state duration. We predicted that the positive feedback field decreases the cycle-to-cycle variability and therefore expected a reduction of the according coefficients of variation. Indeed, such positive feedback increased the rhythmic structure of the slow oscillation (Figure 7F, red data points; coefficients of variations Up: decreased to 86% of control, $p = 0.016$, Down: decreased to 83% of control, $p = 0.016$, $n = 7$; Up duration: increased to 110% of control, $p = 0.031$; Down duration: increased to 110% of control, $p = 0.38$, data not shown). These findings directly support our hypothesis that an EF reflecting ongoing network activity can enhance the very activity that generates it.

If the endogenous field contributes to the rhythmic structure of the slow oscillation as predicted by the above positive feedback experiments, we hypothesized that negative feedback mediated by an activity-dependent field should have the opposite effect on the rhythmic structure by counteracting the endogenous field. We determined the negative feedback from the multiunit signal in real-time with the same set up as for the positive feedback experiments (Figure 7A) yet with two important modifications: (1) the applied EF was of opposite sign and (2) the net field was monitored and the applied EF amplitude was adjusted to

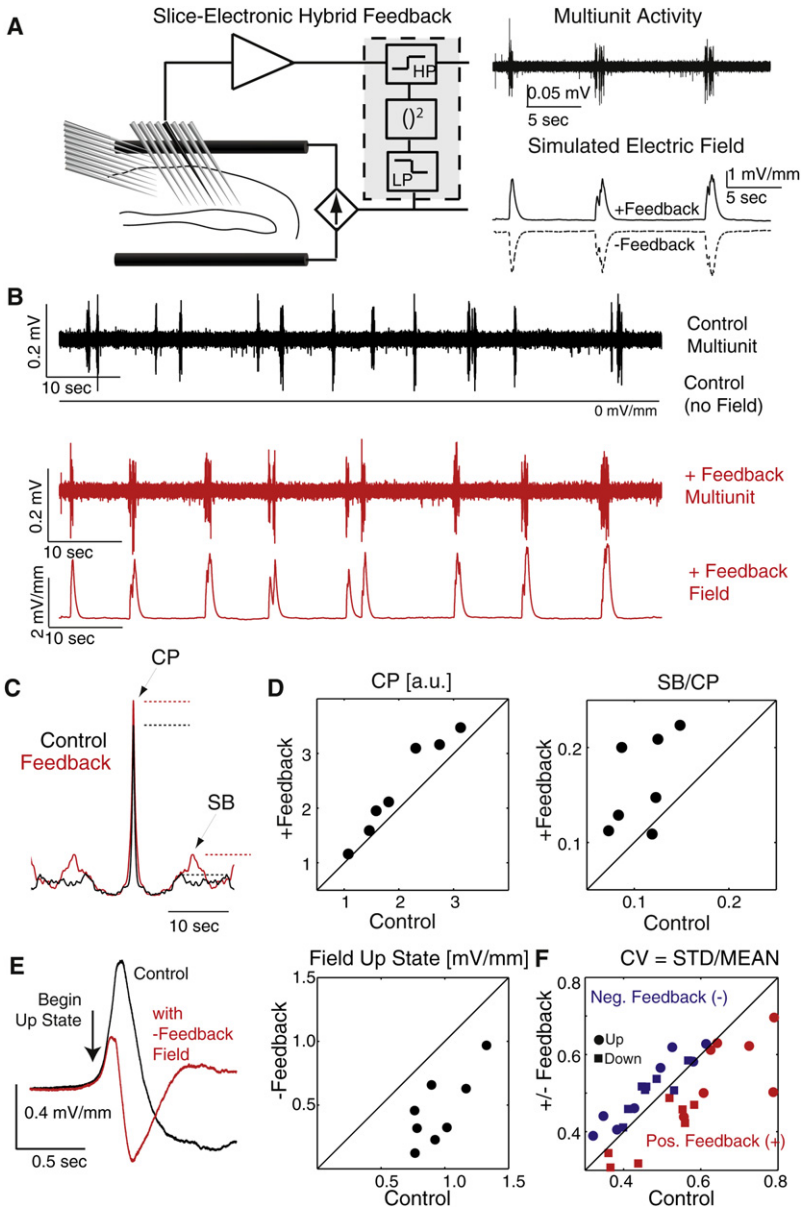


**Figure 7. Positive Feedback EF Enhances, while Negative Feedback EF Diminishes, Slow Oscillation**

Negative feedback field decreases rhythmic structure of the slow oscillation.

(A) Feedback loop is provided by real-time field simulator that provides an EF based on the ongoing multiunit activity. Top: sample multiunit trace. Bottom: simulated EFs.

(B) Representative positive feedback sample experiment. Slow oscillation is more regular in presence of the feedback loop (bottom) than in absence (control, top).

(C) Correlogram of multiunit activity shows both an enhanced central peak (CP) and a more pronounced side-band peak (SB) in presence of the positive feedback (red) in comparison to control condition without feedback (black).

(D) Group data correlograms (n = 7). Activity levels (left) and slow oscillation structure (right) were enhanced in presence of positive feedback field with median relative increase in CP amplitude: 120% (p = 0.016) and SB/CP ratio: 150% (p = 0.031).

(E) Negative feedback experiments. Left: endogenous EF in vitro (black) and EF in presence of negative feedback field (red). Right: positive peak field strength at onset of Up state was reduced to 47% of control (p = 0.0078, n = 8).

(F) Coefficient of variation of both Up and Down state duration decreased in presence of positive feedback EF (red, Up: decreased to 86%, p = 0.016; Down: decreased to 83%, p = 0.016) but increased in presence of negative feedback EF (blue, increased to 111% of control for both Up and Down states, n = 8, p = 0.0039 and p = 0.0078, respectively).

minimize the positive field peak associated with the beginning of the Up state for each experiment (Figure 7E, left; average field waveforms, black: control; red: in presence of negative feedback, average from n = 8 experiments). On average, the positive field peak (E) was reduced to 47% of control by the negative feedback field (Figure 7E, right; $E_{Control}$ = 0.95 ± 0.077 mV/mm, $E_{Feedback}$ = 0.46 ± 0.10 mV/mm, n = 8, p = 0.0078; average peak amplitude of applied feedback field: −0.49 ± 0.068 mV/mm, all values reported as mean ± SEM). The negative feedback field did not achieve complete cancellation of the endogenous EF due to inherent limited ability to predict the endogenous EF waveform from the multiunit firing in real time. In agreement with our hypothesis, we found that negative feedback EFs significantly increased the variability of both the Up and the DOWN state duration as measured by their coefficients of variation (Figure 7F, blue data points; increased to 111% of control for both Up and Down state, p = 0.0039 and p = 0.0078, respectively; Up duration: 100% of control, p = 0.74; Down duration: 101% of control, p = 1.00, data not shown). Therefore, negative feedback increased the cycle-to-cycle variability of the network activation and had the opposite effect of the amplification of the activity-dependent field by positive feedback (Figure 7B). Together, these results suggest that modification of the endogenous EF influences the biophysical mechanisms that shape the rhythmic structure of the slow oscillation.

## Computational Network Model Reproduces Main Features of Feedback Interaction

Finally, we performed network simulations to confirm whether simultaneous small depolarization of all neurons in an active neuronal network is sufficient to explain the experimentally observed enhancement of structured network activity. We chose to use conductance-based two-compartment neuron models because such models closely represent not only the slow oscillation dynamics but also the underlying mechanisms of oscillation generation (interaction of synaptic and intrinsic properties).

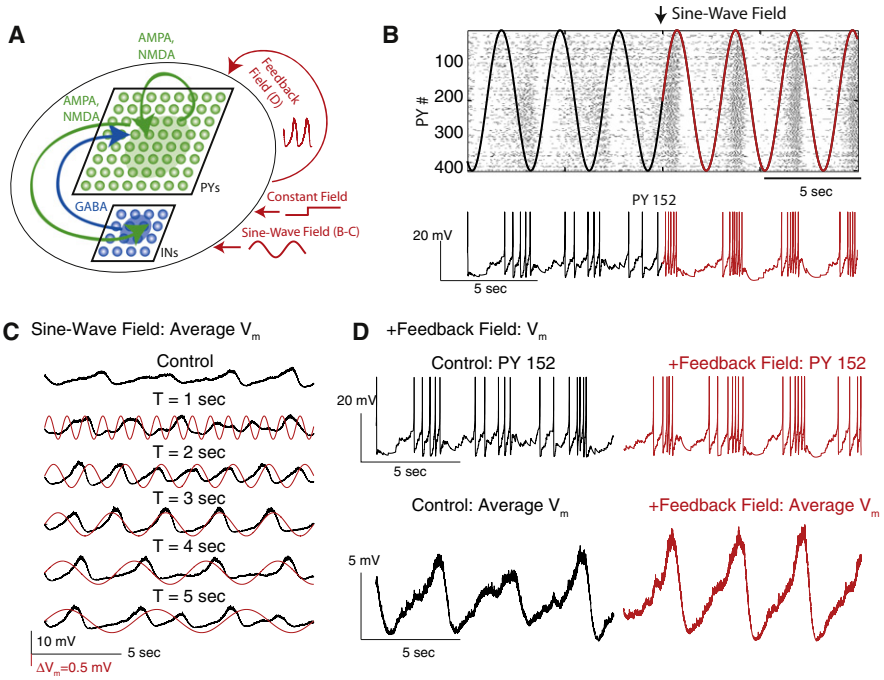


**Figure 8. Computational Network Model Supports Global Small Somatic Depolarization as Mechanism for Activity Modulation by EFs**

(A) Network model with 2D layers of pyramidal neurons (PYs, green) and inhibitory interneurons (INs, blue). Constant, sine-wave and feedback fields were simulated by according somatic current injections into both PYs and INs to cause depolarization that mimicked the measured effect of EFs on the somatic membrane voltage of neurons.

(B) Sine-wave EF entrains slow oscillation. Top: raster plot of PY cell spiking (two-dimensional network structure was linearized for presentation purposes). Red: applied sine-wave EF waveforms. Black: "virtual extension." Bottom: representative PY membrane voltage trace.

(C) Average PY membrane voltage $V_m$. No field applied (control, top) and sine-wave field application with different oscillation periods (second from top to bottom). Entrainment occurs for oscillation periods close to intrinsic oscillation period.

(D) Positive feedback field enhances slow oscillation structure. Top: sample membrane voltage trace (black: control, red: with feedback field). Bottom: average PY $V_m$ (left: control, right: with feedback field).

See also Figure S7.

Our network model consisted of 400 pyramidal cells (PYs) and 64 fast-spiking inhibitory interneurons (INs) arranged into two-dimensional sheets with local synaptic connectivity (Figure 8A; complete model description in Supplemental Experimental Procedures). We modeled the effect of EFs on individual neurons by a small somatic current injection that was calibrated in absence of synaptic connections to cause a depolarization comparable to the values we measured in vitro in response to EF application. Our goal was to determine if such a small but network-wide perturbation of the membrane voltage can explain the effects of EFs we observed in our experiments. Indeed, similar to our experimental data, the application of a small constant current mimicking the effect of the EF on the somatic membrane voltage (resulting in a 0.5 mV depolarization of all neurons on average) caused an acceleration of the slow oscillation frequency (Figure S7A). In qualitative agreement with our experimental data (Figure 3), the oscillation period monotonically decreased for increased constant EF amplitudes in the model (Figure S7B). In further agreement with the experimental data, this acceleration was mediated by a decrease in the Down state duration without change in the Up state duration. We then used the model to test the hypothesis that change in fraction $\alpha$ of cells that are subject to the membrane voltage perturbation $\Delta V_m$ can be counterbalanced by a change in $\Delta V_m$. If true, this relationship further demonstrates that the effect of the weak EFs is amplified by the fact that they act as global perturbations that target entire networks of cells. Indeed, we found that oscillation period and Up and Down state durations exhibited similar dependence on the overall network depolarization (measured as $\alpha^*\Delta V_m$) independent from whether $\alpha$ or $\Delta V_m$ was modulated (Figure S7C).

We next investigated the response of the network model to small amplitude sine-wave perturbations (Figure 8B, top: raster plot of PY cell activity; bottom: sample PY membrane voltage; black: control, red: field applied). In absence of an applied field (control condition), the firing of the PYs exhibit slow fluctuations in firing rate but failed to show pronounced slow oscillation with clearly delimited Up and Down states (Figure 8B, top panel, black "virtual" reference). In presence of the sine-wave field (Figure 8B, top panel, red field waveform, amplitude calibrated to cause 0.5 mV depolarization of all PYs on average), the firing during the Up states became more robust while the Down state activity decreased. Thus, in qualitative agreement with the experimental data, the application of a weak sine-wave field robustly entrained the slow oscillation in the simulations.

Importantly, the oscillation period of the applied field determined the quality of the entrainment of the slow oscillation. For sine-wave EFs with periods (T = 2, 3, 4 s) that were close to the intrinsic network oscillation period (T = 3.1 s), the average PY membrane voltage shows periodic fluctuations (Up states) for each positive cycle of the sine-wave EF. In contrast, fields with pronounced mismatch in oscillation period (T = 1, 5 s) to the intrinsic network period failed to entrain the network (Figure 8C, top trace: average $V_m$ of PYs in absence of applied EF; traces below: average $V_m$ of PYs for sine-wave EFs with periods from T = 1 s to T = 5 s). This preference for matched oscillation period resulted in higher central peak and central peak/sideband peak ratio of the corresponding autocorrelograms for matched oscillation periods (Figure S7D). Last, we tested if the inclusion of the proposed positive feedback loop between neuronal activity and EF enhances the network activity. In these simulations, we included a current that mimicked the effect of an activity-dependent EF ("feedback field"). Specifically, we computed the average PY membrane voltage during the simulation and scaled this value to transform it into a current injection that caused a 0.8 mV depolarization on average in a network without synaptic connectivity. The amplitude of this "EF"-induced depolarization will be smaller in presence of synaptic barrages owing to the decreased input resistance of the neurons. Even so, we found that this positive feedback mechanism facilitated the slow oscillation by enhancing the depolarization and spiking during the Up states and by increasing the hyperpolarization during the Down states (Figure 8D, top: PY membrane voltage traces for control, left, and with feedback field, right; bottom: average membrane voltage for control, left, and with feedback field). Both the CP and the SB/CP ratio were increased (CP: increased to 136% of control, SB/CP: increased to 153% of control) and the coefficients of variations of Up and Down state durations were decreased (Up: decreased to 38% of control, Down: decreased to 22% of control) by the positive feedback field in qualitative agreement with our experimental data. Together, these simulation data provide support that weak but network-wide activity-dependent depolarizations are sufficient to explain the powerful modulating role of EFs on active cortical networks.

## DISCUSSION

Structured neuronal activity operates through the flow of ionic currents, which establish complex endogenous fields (Freeman, 1975; Mitzdorf, 1985; Nunez and Srinivasan, 2006). Little is known about if and how these endogenous EFs may directly affect neocortical network dynamics. We addressed this question by taking advantage of the active neocortical slice preparation that spontaneously exhibits the slow oscillation (Sanchez-Vives and McCormick, 2000). We established that weak constant and sine-wave fields enhance and entrain the slow oscillation. By application of naturalistic in vivo field waveforms in vitro, we determined that fields modulate neocortical network activity with a threshold of $\leq$0.5 mV/mm. These experiments show that the weak EFs generated during normal neocortical activity (which peak at 2–4 mV/mm) have the potential to form a feedback loop that modulates the very activity that generates them. Indeed, we demonstrated that the positive feedback application of activity-dependent EFs in real time to active neocortical slices enhanced the slow oscillation. In further agreement, we showed that a negative feedback field decreased the rhythmic structure of the slow oscillation. Finally, our computational model confirms that such activity-dependent weak yet global perturbations of the membrane voltage can indeed alter the macroscopic network dynamics. Our results therefore support a functional role of the endogenous field in guiding physiological network activity by feedback interaction in neocortex.

### Network-wide Amplification of Weak Membrane Depolarization

EFs cause electric polarization in elongated neuronal structures that are aligned with the field (Chan et al., 1988; Holt and Koch, 1999; McIntyre and Grill, 1999; Nicholson, 1973; Rattay, 1998; Svirskis et al., 1997; Tranchina and Nicholson, 1986). In agreement with previous findings in hippocampus (Bikson et al., 2004; Deans et al., 2007), EFs of up to 4 mV/mm caused a small somatic depolarization of up to about 1 mV in infragranular neurons in neocortex. This depolarization results from local differences in the extracellular and intracellular distribution of ionic charge in response to the imposed extracellular voltage gradient (Figures S2B–S2D). Endogenous EFs exhibit a complex spatial structure that was not matched by the uniform fields applied in this study. However, simulations show that the extracellular potential gradient recorded in vivo may induce a somatic depolarization similar to uniform fields (Figures S1B and S1C; see also Anastassiou et al., 2010). The macroscopic effect of a small perturbation of the membrane voltage depends on the ongoing network dynamics. In case of quiescent neurons in standard conditions in vitro, such a small depolarization is not expected to have any effect on the spiking behavior since spike initiation threshold cannot be reached. In vivo, however, neurons are hardly ever quiescent but are rather involved in the generation of a large number of different activity states that often exhibit complex oscillatory structures (Buzsáki, 2006). Using the active slice preparation, we directly assessed the effect of such weak membrane voltage depolarizations on the ongoing spontaneous network dynamics. We found a stark contrast between the small amplitude of the perturbation at the level of individual neurons and the effect on the macroscopic network dynamics. This amplification of the weak yet global membrane potential perturbation is a direct consequence of the presence of structured network activity. Similar to in vivo, neurons in our cortical slices maintained in vitro were spontaneously active and thus close to or above action potential threshold during periods of network wide activation. In vivo measurements of the relationship between pyramidal cell firing rate as a function of membrane potential reveal that, on average, depolarization of a suprathreshold neuron by even one millivolt will, on average, increase firing rate by 6–9 Hz (Carandini and Ferster, 2000).

### Enhancement of Physiological Activity in Neocortex by Weak Electric Fields

Early studies on the effect of EFs used strong field strengths that may only occur under pathological conditions or special anatomical constellations (Faber and Korn, 1989; Jefferys, 1995). More recent work on the role of weaker EFs in the mammalian brain

mostly focused on rodent hippocampus (Bikson et al., 2004; Deans et al., 2007; Dudek et al., 1986; Fujisawa et al., 2004; Ghai et al., 2000; Grenier et al., 2003; Radman et al., 2007; Snow and Dudek, 1984; Vigmond et al., 1997) that is more prone to nonsynaptic neuronal communication modes (Jefferys and Haas, 1982). Interestingly, recent studies have shown low thresholds of EF amplitudes (within the range of endogenous EF amplitudes) for modulation of pharmacologically- or high-potassium-induced neuronal activity in rodent hippocampal slices (Deans et al., 2007; Francis et al., 2003; Fujisawa et al., 2004). It is unclear, however, if the ability of weak (endogenous) EFs to modulate network dynamics is a general phenomenon or if such effects are restricted to areas of high cell density or to pathological activity (Jefferys, 1995). We therefore sought to determine whether endogenous fields play an active role in neocortex during physiological spontaneous activity. The slow oscillation has several unique properties that made this activity state advantageous for this study. First, the neocortical slow oscillation occurs in slices maintained in a more in vivo-like artificial CSF (Sanchez-Vives and McCormick, 2000). Although the oscillation frequency is lower in vitro, the fundamental properties of bistable membrane dynamics and periodic network-wide activation are maintained (Shu et al., 2003). Second, the slow oscillation closely resembles the activity pattern during slow-wave sleep (Steriade et al., 1993, 2001) which may play an important role in memory consolidation or network homeostasis (Hoffman et al., 2007). An enhancement of the slow oscillation by weak (endogenous) EFs therefore may have functional implications for patterning of activity sequences, interplay between different cortical areas, and local processing. In particular, recent human work showed memory enhancement after exposure to extracranial sinusoidal EFs in the slow oscillation frequency range (Kirov et al., 2009; Marshall et al., 2006). Indeed, our results on amplification of network-wide weak perturbations provide the underlying physiological mechanism of such transcranial electric stimulation. Importantly, the proposed mechanism may shape network dynamics during a broad range of behavioral states since slow structured activity has also been reported in the awake, but quiescent, animal (Crochet and Petersen, 2006).

### Feedback Modulation of Spontaneous Neocortical Network Activity

Our demonstration that active neocortical networks are susceptible to weak constant and sinusoidal fields with amplitudes well within the range of endogenous EF strengths supports the proposed presence of a feedback loop between neural population activity and its endogenous EF. However, the direct study of such a feedback loop between neuronal activity and its endogenous field in vivo remains an experimentally challenging problem. We therefore used (1) naturalistic (in vivo), (2) activity-dependent positive feedback and (3) activity-dependent negative feedback waveforms in the slice preparation. First, macroscopic network oscillations may respond differently to artificial than to ''natural'' field waveforms. We found that uniform EFs with naturalistic waveforms that are less periodic than a sine-wave also had a prominent effect on the network activity. Second, it has so far remained unclear if the observed effects of applied sine-waves translate to the in vivo case where the underlying endogenous field is directly coupled to ongoing network activity and thus by definition ''entrained.'' To address this concern, we developed a hybrid preparation that combined an active slice with analog electronics to reproduce the proposed positive feedback interaction between neural activity and the underlying endogenous field. Similar to the in vivo situation, the EF in these experiments corresponded directly to the ongoing network activity. We found that this positive feedback enhances the slow oscillation. Third, we used negative feedback to demonstrate that an EF of opposite sign to the endogenous field reduces the rhythmic structure of the slow oscillation. Together, these positive and negative feedback experiments represent direct evidence for a functional role of the endogenous EF as a biophysical signal that organizes and structures (oscillatory) network activity. The observed decrease in variability of Up and Down state duration with positive feedback is indicative of enhanced structure and regularity of the slow oscillation. The detailed behavioral and/or network consequences of such a change in activity structure remains to be studied in the future. However, it is expected that decreased variability may enhance cortical network synchronization, which may be useful for a wide variety of neuronal and cognitive tasks (Fries et al., 2001; Lee et al., 2005; Sederberg et al., 2007; Singer, 1993).

In conclusion, our findings show that feedback interaction between structured neuronal activity and endogenous EF can occur in neocortex and may play an important role in shaping normal physiological network activity. The most convincing yet technically unfeasible experiment to confirm our hypothesis would be a manipulation that fully abolishes the endogenous EF in an awake, behaving animal in a noninvasive and specific way. Until such an experiment becomes feasible (if at all), we are limited to integrating the evidence from different types of external field applications to assess the role of endogenous EFs in neocortex as performed in our study. The most conservative conclusion derived from our current work is the susceptibility of active neocortical networks to weak applied EFs. However, we put forward that our data provide important insight beyond the demonstration of the effect of applied weak EFs on physiological neocortical network activity. In particular, our positive feedback field experiments demonstrate that activity-dependent fields have a significant effect on network dynamics. While these fields were still externally applied, they incorporate the most important property of endogenous fields by mimicking the activity-dependent structure of the endogenous fields. In addition, the negative feedback fields reduced the endogenous EFs and caused a decrease in the regularity of the network activity structure in agreement with our hypothesis. Thus, our results propose a reconsideration of (1) pathological neuronal network activity as necessary substrate and (2) rodent hippocampus as necessary location for the occurrence of such a non-synaptic communication mechanism in the mammalian brain. Endogenous EFs can provide a mechanism for rapid orchestration and synchronization of neocortical oscillatory population activity. Therefore, the functional relevance of endogenous fields is eventually defined and limited by our understanding of the behavioral relevance of cortical oscillations in different frequency bands. The oscillatory field potential activity that we studied here, the slow oscillation, is one of the largest

and most spatially synchronized EFs that is known to naturally occur in the neocortex (Destexhe et al., 1999). Although the synchronization of this slow oscillation depends at least in part on corticocortical axonal connections (Amzica and Steriade, 1995), we hypothesize that the endogenous EF may provide an additional mechanism for the synchronization and rapid propagation of the slow oscillation. Field potentials characterized by higher frequencies and smaller amplitudes typically occur on a more local level, such as during sensory processing (Katzner et al., 2009). Whether or not these field potentials may also influence local neuronal network activity is still unknown, although the close apposition of pyramidal cell apical dendrites may provide one avenue for synchronization through local fields (Peters et al., 1997; Peters and Sethares, 1996). Thus, neocortical neuronal networks may not only be defined by their anatomical interconnectivity and the status of the synaptic activity that binds them together (Haider and McCormick, 2009) but also by the spatially and temporally complex EFs in which they are embedded.

## EXPERIMENTAL PROCEDURES

A full description of the methods is published in the Supplemental Information.

### In Vivo Experiments

Male ferrets (*Mustela putorius furo*, 10–14 weeks old) were used for acute in vivo experiments as described previously (Haider et al., 2006). Recordings of extracellular voltage fluctuations were performed with 16 channel silicon recording electrodes (Neuronexus, Ann Arbor, MI) with 100 and 150 μm recording site spacing. An AgCl wire positioned between cranium and retracted muscle was held in electric contact with surrounding tissue by 4% agar and served as reference electrode. Unfiltered signals were preamplified with MPA8I head-stages with gain of 10 (Multi Channel Systems MCS GmbH, Reutlingen, Germany) and then fed into a sixteen-channel amplifier Model 3500 with gain 500 (A-M Systems, Inc., Carlsborg, WA). All recordings were in the dark and with the eyes closed to avoid contamination of the recordings with visually evoked neuronal activity.

### In Vitro Recordings

As previously described (Sanchez-Vives and McCormick, 2000), 400 μm thick coronal slices of ferret (6–8 weeks) visual cortex were maintained in an interface chamber. The horizontal array of extracellular recording electrodes was positioned infragranularly parallel to the underlying white matter; the vertical array was positioned orthogonally such that it spanned layers II/III to VI (or the entire cortical depth in case of the 190 μm spaced array). Recordings of the endogenous EF during slow oscillation in vitro were performed with a linear array of 14 electrodes (115 μm spacing) that spanned the entire cortical depth from pia to white matter. Intracellular recordings from infragranular neurons were performed as previously described (Sanchez-Vives and McCormick, 2000). The true transmembrane voltage deflection caused by the external field was determined by offline subtraction of measurements of the averaged intra- and extracellular voltages in response to constant external fields. Extracellular potential was recorded following loss of the intracellular recording with the electrode immediately outside the recorded neuron.

### Electric Field Application

EFs were applied through two parallel AgCl wires (1 mm diameter) that were arranged such that the slice was subjected to an approximately uniform EF with field lines perpendicular to the cortical surface (Figure S2A). The current to produce the applied EF was generated with an AM Systems 2200 stimulus isolation unit (A-M Systems, Inc., Carlsborg, WA) with the two leads connected to the two field-generating AgCl wires. Field amplitudes were calibrated at the beginning of each experiment by measuring the field potential gradient along the field lines for a sine-wave EF (20 Hz) with an AM Systems 3000 extracellular amplifier (A-M Systems, Inc., Carlsborg, WA) on broadband setting (0.1 Hz–5 kHz, gain 50). The device for generating an EF waveform based on the multiunit activity in real-time was custom-designed and implemented in analog electronics.

### Experimental Design and Data Analysis

Data analysis was performed offline with custom written Matlab scripts (The MathWorks, Inc., Natick, MA). If not noted otherwise, data are reported as median ± SEM and the Wilcoxon signed rank test was used for paired, unparametric tests. Modulation indices were computed as the difference of the value of a variable for a given condition and its value for the control condition (no field applied) divided by their sum. For the phase analysis, the phase of each Up state on all electrodes was determined relative to the applied sine-wave or a "virtual extension" of the sine-wave in case of the control epochs. Phase and phase change histograms are shown for all Up states on all electrodes during all trials of each condition. Absolute phase change ("delta phase," $|\Delta\phi|$) was determined by taking the absolute value of the subtraction of the phase of pairs of consecutive Up states. If $|\Delta\phi|$ assumed a value between 180° and 360°, we subtracted 180° to take the circular nature of the phase measurement into account ($|\Delta\phi|$ ranges between 0° and 180°). Final histograms represent population averages across experiments. Circular statistics implemented in the CircStat MATLAB toolbox (Berens, 2009) were used to assess the resulting histograms (Rayleigh test for nonuniformity, circular variance, linear-circular association). Threshold values for EF amplitude that modulated the slow oscillation were determined by 20–30 applications of a 60 s in vivo EF waveform (interleaved with 60 s control epochs of no applied field).

### Computational Model

The computational model of a network with pyramidal cells (PYs) and fast-spiking inhibitory interneurons (INs) was based on the conductance-based description of ionic currents similar to a previous modeling study on slow oscillation (Compte et al., 2003). All parameters and equations are provided in the Supplemental Experimental Procedures. Excitatory and inhibitory synapses were modeled with first-order kinetics as previously described elsewhere (Fröhlich et al., 2008). The network exhibited a two-dimensional topology with a sheet of PYs (20 × 20 neurons) and a sheet of INs (8 × 8 neurons). The effect of externally applied EFs on the somatic membrane voltage was modeled with a somatic current injection that caused a small membrane voltage deflection that was comparable to what was measured in vitro. The feedback interaction between neuronal activity and EF was modeled with an activity-dependent current injection into all cells in the network. Specifically, the average membrane voltage of all PYs was computed online during the simulation. This value was then scaled such that the resulting injected current caused a 0.8 mV depolarization in PYs without synaptic connectivity on average.

## SUPPLEMENTAL INFORMATION

Supplemental Information includes seven figures, one table, and Supplemental Experimental Procedures and can be found with this article online at doi:10.1016/j.neuron.2010.06.005.

## ACKNOWLEDGMENTS

This work was supported by the National Institutes of Health. F.F. was funded by the Swartz Foundation. We thank Kristy Sundberg for her help with the in vivo experiments and her valuable input on earlier versions of this manuscript. We thank Carlos Maureira for input on an early version of this manuscript and Tatiana Engel for helpful discussions.

Accepted: June 1, 2010
Published: July 14, 2010

## REFERENCES

Amzica, F., and Steriade, M. (1995). Disconnection of intracortical synaptic linkages disrupts synchronization of a slow oscillation. J. Neurosci. *15*, 4658–4677.

Anastassiou, C.A., Montgomery, S.M., Barahona, M., Buzsáki, G., and Koch, C. (2010). The effect of spatially inhomogeneous extracellular electric fields on neurons. J. Neurosci. *30*, 1925–1936.

Berens, P. (2009). CircStat: A MATLAB toolbox for circular statistics. J. Stat. Softw. *31*, 1–21.

Berens, P., Keliris, G.A., Ecker, A.S., Logothetis, N.K., and Tolias, A.S. (2008). Feature selectivity of the gamma-band of the local field potential in primate primary visual cortex. Front Neurosci *2*, 199–207.

Bikson, M., Inoue, M., Akiyama, H., Deans, J.K., Fox, J.E., Miyakawa, H., and Jefferys, J.G. (2004). Effects of uniform extracellular DC electric fields on excitability in rat hippocampal slices in vitro. J. Physiol. *557*, 175–190.

Buzsáki, G. (2006). Rhythms of the Brain (Oxford: Oxford University Press).

Carandini, M., and Ferster, D. (2000). Membrane potential and firing rate in cat primary visual cortex. J. Neurosci. *20*, 470–484.

Chan, C.Y., Hounsgaard, J., and Nicholson, C. (1988). Effects of electric fields on transmembrane potential and excitability of turtle cerebellar Purkinje cells in vitro. J. Physiol. *402*, 751–771.

Compte, A., Sanchez-Vives, M.V., McCormick, D.A., and Wang, X.J. (2003). Cellular and network mechanisms of slow oscillatory activity (<1 Hz) and wave propagations in a cortical network model. J. Neurophysiol. *89*, 2707–2725.

Crochet, S., and Petersen, C.C. (2006). Correlating whisker behavior with membrane potential in barrel cortex of awake mice. Nat. Neurosci. *9*, 608–610.

Deans, J.K., Powell, A.D., and Jefferys, J.G. (2007). Sensitivity of coherent oscillations in rat hippocampus to AC electric fields. J. Physiol. *583*, 555–565.

Destexhe, A., Contreras, D., and Steriade, M. (1999). Spatiotemporal analysis of local field potentials and unit discharges in cat cerebral cortex during natural wake and sleep states. J. Neurosci. *19*, 4595–4608.

Dudek, F.E., Snow, R.W., and Taylor, C.P. (1986). Role of electrical interactions in synchronization of epileptiform bursts. Adv. Neurol. *44*, 593–617.

Faber, D.S., and Korn, H. (1989). Electrical field effects: their relevance in central neural networks. Physiol. Rev. *69*, 821–863.

Francis, J.T., Gluckman, B.J., and Schiff, S.J. (2003). Sensitivity of neurons to weak electric fields. J. Neurosci. *23*, 7255–7261.

Freeman, W.J. (1975). Mass Action in the Nervous System (New York: Academic Press).

Fries, P., Reynolds, J.H., Rorie, A.E., and Desimone, R. (2001). Modulation of oscillatory neuronal synchronization by selective visual attention. Science *291*, 1560–1563.

Fries, P., Womelsdorf, T., Oostenveld, R., and Desimone, R. (2008). The effects of visual stimulation and selective visual attention on rhythmic neuronal synchronization in macaque area V4. J. Neurosci. *28*, 4823–4835.

Fröhlich, F., Bazhenov, M., and Sejnowski, T.J. (2008). Pathological effect of homeostatic synaptic scaling on network dynamics in diseases of the cortex. J. Neurosci. *28*, 1709–1720.

Fujisawa, S., Matsuki, N., and Ikegaya, Y. (2004). Chronometric readout from a memory trace: gamma-frequency field stimulation recruits timed recurrent activity in the rat CA3 network. J. Physiol. *561*, 123–131.

Gail, A., Brinksmeyer, H.J., and Eckhorn, R. (2004). Perception-related modulations of local field potential power and coherence in primary visual cortex of awake monkey during binocular rivalry. Cereb. Cortex *14*, 300–313.

Ghai, R.S., Bikson, M., and Durand, D.M. (2000). Effects of applied electric fields on low-calcium epileptiform activity in the CA1 region of rat hippocampal slices. J. Neurophysiol. *84*, 274–280.

Grenier, F., Timofeev, I., Crochet, S., and Steriade, M. (2003). Spontaneous field potentials influence the activity of neocortical neurons during paroxysmal activities in vivo. Neuroscience *119*, 277–291.

Haider, B., and McCormick, D.A. (2009). Rapid neocortical dynamics: cellular and network mechanisms. Neuron *62*, 171–189.

Haider, B., Duque, A., Hasenstaub, A.R., and McCormick, D.A. (2006). Neocortical network activity in vivo is generated through a dynamic balance of excitation and inhibition. J. Neurosci. *26*, 4535–4545.

Hoffman, K.L., Battaglia, F.P., Harris, K., MacLean, J.N., Marshall, L., and Mehta, M.R. (2007). The upshot of up states in the neocortex: from slow oscillations to memory formation. J. Neurosci. *27*, 11838–11841.

Holt, G.R., and Koch, C. (1999). Electrical interactions via the extracellular potential near cell bodies. J. Comput. Neurosci. *6*, 169–184.

Jefferys, J.G. (1995). Nonsynaptic modulation of neuronal activity in the brain: electric currents and extracellular ions. Physiol. Rev. *75*, 689–723.

Jefferys, J.G., and Haas, H.L. (1982). Synchronized bursting of CA1 hippocampal pyramidal cells in the absence of synaptic transmission. Nature *300*, 448–450.

Katzner, S., Nauhaus, I., Benucci, A., Bonin, V., Ringach, D.L., and Carandini, M. (2009). Local origin of field potentials in visual cortex. Neuron *61*, 35–41.

Kirov, R., Weiss, C., Siebner, H., Born, J., and Marshall, L. (2009). Slow oscillation electrical brain stimulation during waking promotes EEG theta activity and memory encoding. Proc. Natl. Acad. Sci. USA *106*, 15460–15465.

Lee, H., Simpson, G.V., Logothetis, N.K., and Rainer, G. (2005). Phase locking of single neuron activity to theta oscillations during working memory in monkey extrastriate visual cortex. Neuron *45*, 147–156.

Liu, J., and Newsome, W.T. (2006). Local field potential in cortical area MT: stimulus tuning and behavioral correlations. J. Neurosci. *26*, 7779–7790.

Marshall, L., Helgadóttir, H., Mölle, M., and Born, J. (2006). Boosting slow oscillations during sleep potentiates memory. Nature *444*, 610–613.

McIntyre, C.C., and Grill, W.M. (1999). Excitation of central nervous system neurons by nonuniform electric fields. Biophys. J. *76*, 878–888.

Mitzdorf, U. (1985). Current source-density method and application in cat cerebral cortex: investigation of evoked potentials and EEG phenomena. Physiol. Rev. *65*, 37–100.

Nicholson, C. (1973). Theoretical analysis of field potentials in anisotropic ensembles of neuronal elements. IEEE Trans. Biomed. Eng. *20*, 278–288.

Niedermeyer, E., and Lopes da Silva, F.H. (2005). Electroencephalography: Basic Principles, Clinical Applications, and Related Fields, Fifth Edition (Philadelphia: Lippincott Williams & Wilkins).

Nunez, P.L., and Srinivasan, R. (2006). Electric Fields of the Brain: The Neurophysics of EEG, Second Edition (Oxford: Oxford University Press).

Pesaran, B., Pezaris, J.S., Sahani, M., Mitra, P.P., and Andersen, R.A. (2002). Temporal structure in neuronal activity during working memory in macaque parietal cortex. Nat. Neurosci. *5*, 805–811.

Peters, A., and Sethares, C. (1996). Myelinated axons and the pyramidal cell modules in monkey primary visual cortex. J. Comp. Neurol. *365*, 232–255.

Peters, A., Cifuentes, J.M., and Sethares, C. (1997). The organization of pyramidal cells in area 18 of the rhesus monkey. Cereb. Cortex *7*, 405–421.

Pikovsky, A., Rosenblum, M., and Kurths, J. (2001). Synchronization: A Universal Concept in Nonlinear Sciences (Cambridge: Cambridge University Press).

Radman, T., Su, Y., An, J.H., Parra, L.C., and Bikson, M. (2007). Spike timing amplifies the effect of electric fields on neurons: implications for endogenous field effects. J. Neurosci. *27*, 3030–3036.

Rattay, F. (1998). Analysis of the electrical excitation of CNS neurons. IEEE Trans. Biomed. Eng. *45*, 766–772.

Riedner, B.A., Vyazovskiy, V.V., Huber, R., Massimini, M., Esser, S., Murphy, M., and Tononi, G. (2007). Sleep homeostasis and cortical synchronization: III. A high-density EEG study of sleep slow waves in humans. Sleep *30*, 1643–1657.

Sanchez-Vives, M.V., and McCormick, D.A. (2000). Cellular and network mechanisms of rhythmic recurrent activity in neocortex. Nat. Neurosci. *3*, 1027–1034.

Schroeder, C.E., Mehta, A.D., and Givre, S.J. (1998). A spatiotemporal profile of visual system activation revealed by current source density analysis in the awake macaque. Cereb. Cortex *8*, 575–592.

Sederberg, P.B., Schulze-Bonhage, A., Madsen, J.R., Bromfield, E.B., McCarthy, D.C., Brandt, A., Tully, M.S., and Kahana, M.J. (2007). Hippocampal and neocortical gamma oscillations predict memory formation in humans. Cereb. Cortex *17*, 1190–1196.

Shu, Y., Hasenstaub, A., Badoual, M., Bal, T., and McCormick, D.A. (2003). Barrages of synaptic activity control the gain and sensitivity of cortical neurons. J. Neurosci. *23*, 10388–10401.

Singer, W. (1993). Synchronization of cortical activity and its putative role in information processing and learning. Annu. Rev. Physiol. *55*, 349–374.

Snow, R.W., and Dudek, F.E. (1984). Electrical fields directly contribute to action potential synchronization during convulsant-induced epileptiform bursts. Brain Res. *323*, 114–118.

Spinks, R.L., Kraskov, A., Brochier, T., Umilta, M.A., and Lemon, R.N. (2008). Selectivity for grasp in local field potential and single neuron activity recorded simultaneously from M1 and F5 in the awake macaque monkey. J. Neurosci. *28*, 10961–10971.

Steriade, M., and Amzica, F. (1996). Intracortical and corticothalamic coherency of fast spontaneous oscillations. Proc. Natl. Acad. Sci. USA *93*, 2533–2538.

Steriade, M., Nuñez, A., and Amzica, F. (1993). A novel slow (< 1 Hz) oscillation of neocortical neurons in vivo: depolarizing and hyperpolarizing components. J. Neurosci. *13*, 3252–3265.

Steriade, M., Timofeev, I., and Grenier, F. (2001). Natural waking and sleep states: a view from inside neocortical neurons. J. Neurophysiol. *85*, 1969–1985.

Svirskis, G., Baginskas, A., Hounsgaard, J., and Gutman, A. (1997). Electrotonic measurements by electric field-induced polarization in neurons: theory and experimental estimation. Biophys. J. *73*, 3004–3015.

Taylor, K., Mandon, S., Freiwald, W.A., and Kreiter, A.K. (2005). Coherent oscillatory activity in monkey area v4 predicts successful allocation of attention. Cereb. Cortex *15*, 1424–1437.

Tranchina, D., and Nicholson, C. (1986). A model for the polarization of neurons by extrinsically applied electric fields. Biophys. J. *50*, 1139–1156.

Vigmond, E.J., Perez Velazquez, J.L., Valiante, T.A., Bardakjian, B.L., and Carlen, P.L. (1997). Mechanisms of electrical coupling between pyramidal cells. J. Neurophysiol. *78*, 3107–3116.

Wilke, M., Logothetis, N.K., and Leopold, D.A. (2006). Local field potential reflects perceptual suppression in monkey visual cortex. Proc. Natl. Acad. Sci. USA *103*, 17507–17512.